

COLOR-GUIDED FLYING PIXEL CORRECTION IN DEPTH IMAGES

Ekamresh Vasudevan* Shashank N. Sridhara* Eduardo Pavez* Antonio Ortega*
Raghavendra Singh† Srinath Kalluri†

*Dept of Electrical and Computer Engineering, University of Southern California,
†OYLA Inc.

ABSTRACT

We present a novel method to correct flying pixels within data captured by Time-of-flight (ToF) sensors. Flying pixel (FP) artifacts occur when signals from foreground and background objects reach the same sensor pixel, leading to a confident yet incorrect depth estimation in space—floating between two objects. Commercial RGB-D cameras have a complementary setup consisting of ToF sensors to capture depth in addition to RGB cameras. We propose a novel method to correct FPs by leveraging the aligned RGB and depth image in such RGB-D cameras to estimate the true depth values of FPs. Our method defines a 3D neighborhood around each point, representing a “field of view” that mirrors the acquisition process of ToF cameras. We propose a two-step iterative correction algorithm in which the FPs are first identified. Then, we estimate the true depth value of FPs by solving a least-squares optimization problem. Experimental results show that our proposed algorithm estimates the depth value of FPs as accurately as other algorithms in the literature.

Index Terms— flying pixels, Time of Flight cameras, RGB+D

1. INTRODUCTION

Advancements in sensor technology, along with a wide range of applications, including autonomous mobile robotics [4, 13], 3D reconstruction [8], and object localization [24], have made time-of-flight (ToF) cameras popular in 3D vision tasks. ToF cameras use compact, low-cost, efficient depth sensors to capture the 3D information of a scene by sending out periodically modulated light and then inferring depth by measuring the reflection [14, 7]. However, these cameras suffer from problems that limit their practical use.

One of the primary issues that affect ToF cameras is that of flying pixels (FPs) [7], which form due to sensing pipeline limitations. FPs are incorrect depth measurements occurring when light from both a foreground and background object is processed by the same sensor pixel, leading to a mixed depth measurement [1] (see Figure 1). The presence of FPs affects downstream 3D vision tasks such as depth upsampling, object localization, and registration [2, 16, 7, 20]. Therefore, resolving FPs within depth maps captured by ToF cameras is crucial. Existing works that deal with the FP problem focus on mitigating them during acquisition [1]. Others have focused on FP identification [19], which can be used to remove FPs from data [21, 5, 9] or to correct them [20, 18].

The advent of ToF sensors has enabled the development of compact cameras that capture both color and depth. These RGB-D cameras, such as Kinect, generally capture high-resolution RGB and low-resolution depth information separately and calibrate them to align depth and RGB images onto the same image plane [23].

Recently, novel cameras have been developed to overcome calibration issues. For example, the *Oyla* camera [22] can capture both

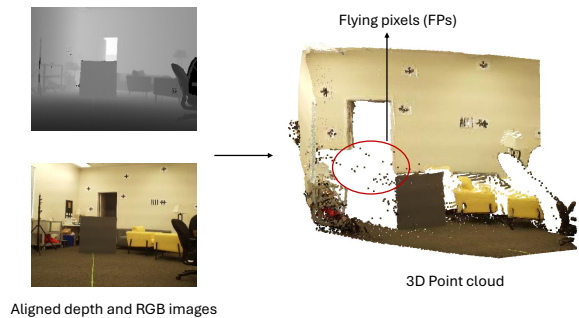


Fig. 1: Aligned RGB and depth images from *Oyla* dataset. 3D point cloud is obtained using the camera intrinsic matrix. Flying pixels can be observed between the foreground and background objects.

color and depth simultaneously through a single lens, thereby avoiding the computationally expensive calibration process (alignment) and loss of information. The result is a well-aligned, high-resolution color and low-resolution depth pair for every capture.

While depth images are prone to measurement errors, such as flying pixels, color images are more accurate due to higher resolution sensors. Therefore, for well-aligned high-resolution RGB and low-resolution depth, the color information can be used to enhance the quality of depth maps [16, 11, 3].

In this work, we assume that aligned high-resolution RGB and low-resolution depth are available, and we focus on *correcting* flying pixels based on the observation that pixels with similar color values are likely to belong to the same surface and, therefore, can be used to correct FPs.

While most existing techniques correct depth by using 2D neighborhoods and depth processing, we propose using a novel 3D neighborhood around each flying pixel and only use points within this 3D region to correct depth (refer to Figure 2). Specifically, given the camera’s intrinsic parameters, we convert the depth image into a 3D point cloud and construct a 3D neighborhood for each point (depth pixel) that provides a reasonable abstraction of the pixel field of view (FoV) principle [17]. We also constrain the optimization so that the corrected depth value lies on the line between the camera and the flying pixel to follow the line of sight principle within ToF cameras [6].

We propose a two-step iterative algorithm that first identifies FPs and then estimates the true depth value of the detected FPs using the corresponding aligned RGB image. We specifically minimize the sum of weighted squared errors between the given depth value and the neighboring depth values within the FP’s FoV. The

weights are calculated based on the color difference between the pixels, thereby encouraging the pixels with similar color values to have similar depth values.

1.1. Related Work

Given their prevalence within ToF cameras, methods have been proposed to address FPs, including mitigation and post-processing approaches. *Mitigation* techniques focus on preventing FPs from generating during acquisition. A learning-based approach to mitigate FPs learns microlens masks for every sensor pixel, which modifies the sub-pixel aperture and effectively blocks one of the signals [1]. *Post-processing* techniques, on the other hand, deal with data that already contains FPs. A method to identify FPs with confidence, but without correcting them, has been proposed [19]. ToF cameras, e.g., the Kinect v2, apply spatial filters to remove FPs [21], and post-processing methods propose similar removal [5, 9]. However, removing FPs, rather than correcting them, results in lower-resolution objects in 3D (fewer points), which may be undesirable since originally captured point clouds are already low-resolution. Some approaches propose correcting flying pixels using spatial information and neighborhoods. However, this approach does not necessarily move a flying pixel to the correct object since the color is not considered [20, 18, 17]. Smoothing techniques such as the bilateral filter are used to enforce consistency within depth images by referencing high-resolution RGB images [12]. However, these methods use 2D neighborhoods and can duplicate FPs when not applied selectively.

We organize the rest of the paper as follows. Section 2 describes ToF sensor preliminaries. Following this, Section 3 presents the proposed flying pixel correction algorithm. Experiments and conclusions are in Section 4 and Section 5 respectively.

2. RGB-D CAMERA SENSOR MODEL

In what follows, we denote 2D pixel coordinates by (u, v) . The depth value at location (u, v) is denoted as d_{uv} . A point in the 3D point cloud is denoted by $\mathbf{p}_i = [x_i, y_i, z_i]^T$. \mathbf{M} denotes the intrinsic camera matrix.

RGB-D cameras such as Kinect-v2 use amplitude-modulated continuous wave (AMCW) ToF cameras for depth acquisition and the standard RGB camera [23]. AMCW ToF cameras operate by sending periodic amplitude-modulated light and measuring the phase difference of the returned light to infer depth [1]. In principle, a received light wave is bounced back from a single point on the object as the light cannot illuminate any point beyond that object. Therefore, it is not possible to have more than one point on the same line of sight [6]. Due to the diverging measurement volume, each sensor pixel has a field of view, which projects out as a series of non-intersecting cones [6] (refer to Figure 2). Given the horizontal and vertical FoV, F_h and F_v of a camera, the pixel FoV is obtained by $(\frac{F_h}{M}, \frac{F_v}{N})$, where M and N are the width and height of the image (in pixels), respectively. Sometimes, a single sensor pixel’s FoV may capture two reflected IR signals. This effect typically occurs at depth discontinuities, where one signal originates from a foreground object and another from the background. Due to the camera aperture’s inability to block one of the received signals, a mixed depth reading is measured [1]. The result is a distance measurement that is a scaled combination of two separate objects’ depths. These flying pixels are confident depth measurements at incorrect depths [1]. The only indication that their depth might be incorrect comes from noticing that, visually, FPs appear as points floating in 3D space away from any particular object.

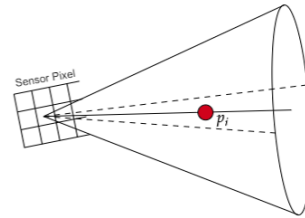


Fig. 2: Field of View Principle

Kinect v2 consists of two lenses in a single system, one for capturing color and one for depth. This results in a difference in the FoV between the captured RGB and depth images. As a result, calibration is necessary to “align” the two images so they look at the same view. On the other hand, novel RGB-D cameras, such as those developed by *Oyla*, employ a single lens to capture RGB and depth data [22]. The camera receives visible and infrared light through the same lens, which a dichroic mirror then splits, letting only a small bandwidth of light (IR signal) pass. The remaining signal is reflected onto an RGB sensor. This implementation enables the RGB and depth images to look at the same field of view, streamlining the acquisition pipeline and generating high-quality, aligned data. More precisely, in the *Oyla* camera, for each depth pixel d_{uv} , there are 36 corresponding pixels in the higher resolution RGB image, forming a color patch $\mathbf{c}_i \in \mathbb{R}^{6 \times 6 \times 3}$.

Given that our method proposes using a novel neighborhood in 3D, it is necessary to have 3D information for every point within the depth map. Since a depth image encodes the distance between a point and the camera at every pixel, depth images can be converted to a 3D point cloud with the intrinsic camera matrix \mathbf{M} . The conversion from 2D homogenous coordinates to a 3D point in the camera frame is given by,

$$[x_i, y_i, z_i]^T = d_{uv} \cdot \mathbf{M}^{-1} [u, v, 1]^T \quad (1)$$

where (u, v) denotes pixel coordinates, d_{uv} is the depth value of the pixel (u, v) and (x_i, y_i, z_i) is the corresponding 3D point.

3. PROPOSED FLYING PIXELS CORRECTION ALGORITHM

Our approach to correcting flying pixels involves a two-step iterative algorithm. First, the algorithm identifies flying pixels within a depth map by generating a score for every depth measurement. We apply a threshold to this metric to identify FPs. Once identified, these pixels are corrected using our proposed method. The corrected depth map is then reprocessed by the algorithm to identify any remaining flying pixels - using the same threshold as before. This iterative method ensures that flying pixels, which may have been missed due to initial thresholding or were sub-optimally corrected during the prior passes, are corrected. It also allows the algorithm to use previously corrected FPs as good points to correct neighboring FPs, resulting in a more accurate depth map (see Figure 3).

3.1. Identification of Flying Pixels

The sum of absolute differences (SAD) of pixel values is often used for quantifying the homogeneity of regions within images [15]. We use SAD to identify flying pixels, replicating the method used in

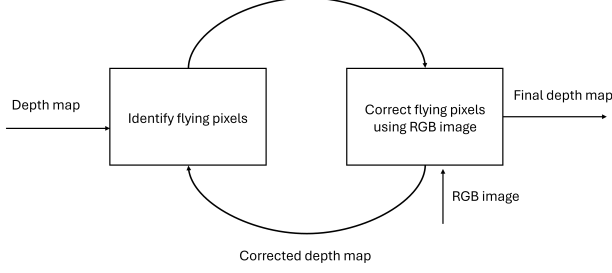


Fig. 3: Iterative Flying Pixel Correction

[20]. For every pixel within a depth image, we construct a 2D window centered on a pixel d_{uv} and calculate the sum of absolute differences between d_{uv} and its neighboring pixels within the window. The SAD score of d_{uv} is given by

$$s(u, v) = \sum_{n=1}^{ws} \sum_{m=1}^{ws} |d_{uv} - d_{nm}| \quad (2)$$

where ws denotes window size, and (n, m) is the index of a neighboring pixel in the window. Since FPs do not belong to a particular object, their depth measurements vary significantly from depth measurements within the window, tending to a high SAD score. We classify the top τ percent of SAD scores as flying pixels (we use $\tau = 5$).

3.2. Field of View Neighborhood

To effectively correct the value of a flying pixel, it is essential to leverage reliable neighborhood information from surrounding data points. Traditional methods primarily utilize a 2D neighborhood for this purpose, aiming to refine the noisy estimates [20, 12, 18]. However, to more accurately reflect the camera’s acquisition process, we adopt the pixel FoV principle discussed in Section 2 to define our neighborhood (see Figure 2). This allows us to identify the foreground and background objects that caused an incorrect depth reading.

Assuming the camera is at the origin, $[0, 0, 0]$, we define a line, ℓ_i , in 3D space, that passes through the camera location and the point \mathbf{p}_i (flying pixel) to be corrected. We constrain the corrected position, $\hat{\mathbf{p}}_i$, of the flying pixel \mathbf{p}_i to be a point on the line ℓ_i

$$\hat{\mathbf{p}}_i = \mathbf{p}_i + t\mathbf{r}_i \quad (3)$$

where t is a scaling factor, and \mathbf{r}_i is a unit vector along this line. By constraining $\hat{\mathbf{p}}_i$ in this manner, we ensure the corrected pixel belongs to the camera line of sight. We apply this constraint since the two objects from which the mixed signal originates are near the line of sight ℓ_i .

3.3. Optimization Framework for Correction

Given a list of candidate flying pixels from the identification step (Section 3.1), we obtain their corresponding 3D positions \mathbf{p}_i using the 2D to 3D coordinate transformation in (1). Given a 3D neighborhood around a candidate point \mathbf{p}_i as described in Section 3.2, we define an objective function to estimate the true position as

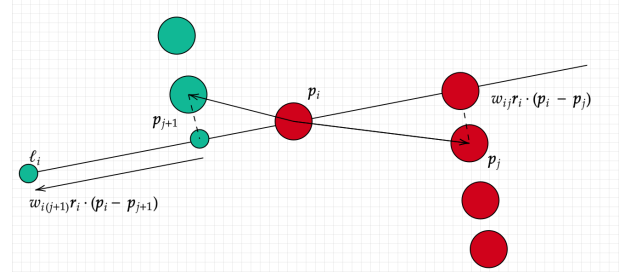


Fig. 4: Geometric interpretation of the closed-form solution of the objective function. The red circle at \mathbf{p}_i represents the flying pixel (FP). This pixel lies along the principal line ℓ_i , which denotes the line of sight of the camera. The green and red circles are neighboring pixels \mathbf{p}_j , with red indicating neighbors that share the same color as the FP in the reference RGB image, and green indicating neighbors of a different color.

$$\hat{\mathbf{p}}_i = \arg \min_{\hat{\mathbf{p}}_i} \sum_{j \in \mathcal{F}(i)} w_{ij} (\hat{\mathbf{p}}_i - \mathbf{p}_j)^2$$

such that $\hat{\mathbf{p}}_i = \mathbf{p}_i + t\mathbf{r}_i$ (4)

where

$$w_{ij} = \exp\left(-\frac{\|\mathbf{c}_i - \mathbf{c}_j\|_2^2}{2\sigma_c^2}\right) \quad (5)$$

The objective function in (4) aims to minimize the weighted squared distance between the flying pixel point \mathbf{p}_i and its neighbors $\mathcal{F}(i)$ in the 3D FoV neighborhood. The weights w_{ij} are calculated based on the color difference, thereby effectively encouraging the point \mathbf{p}_i to move towards its neighbors with similar color values. Since the RGB image generated by the *Oyla* camera is six times the resolution of the depth, we average the squared L_2 -norm between the color patch \mathbf{c}_i and neighbor patch \mathbf{c}_j . Since the directional vector \mathbf{r}_i is constant, we can equivalently write the objective function as

$$t^* = \arg \min_t \sum_{j \in \mathcal{F}(i)} (w_{ij} (\mathbf{p}_i + t\mathbf{r}_i - \mathbf{p}_j)^2) \quad (6)$$

which is in the form of a standard ordinary least squares (OLS) problem, leading to the closed-form solution

$$t^* = -\frac{\sum_{j \in \mathcal{F}(i)} w_{ij} \mathbf{r}_i^\top (\mathbf{p}_i - \mathbf{p}_j)}{\sum_{j \in \mathcal{F}(i)} w_{ij}} \quad (7)$$

This closed-form solution computes the error vectors $(\mathbf{p}_i - \mathbf{p}_j)$, $\forall j \in \mathcal{F}(i)$ and projects them in the direction of the principal line ℓ_i represented by \mathbf{r}_i , with each projection given a weighting that depends on the color difference $(\mathbf{c}_i - \mathbf{c}_j)$. The geometric interpretation is visualized in Figure 4. The factor t quantifies the required adjustment along ℓ_i from the FP’s initial position, given its neighbors’ color and depth values. The corrected depth value \hat{d}_{uv} corresponding to the new position of the point $\hat{\mathbf{p}}_i$ can be obtained by 3D to 2D coordinate conversion using (1).

We perform the correction described in (7) on all the candidate flying pixels obtained from the identification step. We exclude the other candidate flying pixels from the FoV neighborhood during optimization. We treat every iteration as independent, and do not note which pixels have been previously identified as FPs. This allows us

Algorithm 1 Iterative Flying Pixel Correction

```
1: procedure FP_CORRECTION(depth, rgb, ws,  $\tau$ )
2:   for  $k \leftarrow 1$  to iterations do
3:      $s_{uv} \leftarrow \text{get\_sad}(\text{depth}, \text{ws}), \forall u, v$ 
4:      $\text{cloud} \leftarrow \text{get\_point\_cloud}(\text{depth}, \text{rgb})$ 
5:      $\mathcal{O} \leftarrow \text{threshold}(s_{uv}, \tau), \forall u, v$   $\triangleright$  List of outliers
6:     for  $i \leftarrow 1$  to all FPs in  $\mathcal{O}$  do
7:        $\mathcal{F}(i) \leftarrow \text{get\_fov}(p_i, \text{cloud})$ 
8:        $\hat{p}_i \leftarrow \text{get\_optimal\_point}(\mathcal{F}(i), \text{rgb})$ 
9:        $\hat{d}_{uv} \leftarrow \hat{p}_i$ 
10:    end for
11:  end for
12: end procedure
```

to use FPs corrected in previous iterations to fix sub-optimal corrections. The overall correction algorithm is given in Algorithm 1¹.

Scene	Native		Neighbor Distance		Bilateral Filter		Proposed Method	
	RMSE	MAE	RMSE	MAE	RMSE	MAE	RMSE	MAE
corridor_03	106.16	2.38	81.21	1.35	73.12	1.60	54.51	1.33
restaurant_06	26.89	0.53	26.82	0.41	21.37	0.43	23.33	0.42
restaurant_09	37.51	1.17	34.95	0.88	33.03	0.91	28.77	0.91
lectureroom_02	17.40	0.36	13.83	0.41	9.88	0.19	8.51	0.19
livingroom_02	95.82	2.35	56.92	1.25	71.32	1.62	50.12	1.13

Table 1: Average RMSE and MAE between ground truth and depth maps corrected by various methods

4. EXPERIMENTS

4.1. Synthetic Data

We first conduct experiments on synthetic data with simulated flying pixels. Specifically, we utilize the *iBims-1* dataset, which provides high-resolution ground truth depth along with aligned RGB data [10]. We randomly select a percentage of edge pixels from the corresponding edge maps provided in the dataset. Next, we construct a 2D window around the selected edge pixels, select the maximum and minimum depth measurements within this window, and re-assign the selected pixels’ depth to a random value within this range. This process effectively moves reliable edge pixels to unreliable depths between objects - mimicking flying pixels (see Figure 5). While experiments on this synthetic data yield excellent results, we emphasize the outcomes observed within later experiments, as they contain real flying pixels.



Fig. 5: Visualization of ground truth point cloud with and without generated flying pixels

¹https://github.com/STAC-USC/Color_Guided_Flying_Pixel_Correction_in_Depth_Images

We compare our proposed method with the neighbor distance filter proposed in [20] and a bilateral filter commonly used for depth completion [16, 12]. We apply each correction algorithm to the same set of flying pixels within the data and remove identified FPs from the neighborhood used for correction.

In these experiments, the methods require various parameters. For the neighbor distance method and bilateral filter, we set the window size as $ws = 5$. For both the bilateral filter and the proposed method, we set color variance to $\sigma_c = 0.1$ and the spatial variance in the bilateral filter to $\sigma_s = 0.3$. Given the intrinsic parameters of the *Oyla* camera, we calculate that each pixel has a FoV of $.1375^\circ \times .1375^\circ$. While this is the native field of view pixel, we can increase this value to provide more neighborhood information to correct every flying pixel. In our experiments, we increase the FoV in each direction by a factor of $\epsilon = 5$ to a size of $.6875^\circ \times .6875^\circ$.

After applying all three correction methods to the data, our proposed method performs well against the alternatives. As shown in Table 1, the proposed method achieves RMSE and MAE values that are competitive with or better than both filters. With the ground truth indicated by blue line segments, our results show that our correction method successfully aligns pixels to the correct object surfaces, as illustrated in Figure 6. Although the neighbor distance method visually appears to eliminate flying pixels effectively, it results in the highest RMSE and MAE among all algorithms. This discrepancy is likely due to the method’s reliance solely on depth information, which causes flying pixels to be inaccurately projected onto incorrect objects, leading to significant displacement from their true positions in the ground truth. This reflects the unreliability of using only depth information to characterize flying pixel corrections.

4.2. Oyla Data

We conduct our primary experiments on real-world data generated by the *Oyla* camera². This dataset is distinctive due to its extensive range and the inclusion of various outdoor scenes. By leveraging the camera’s wide range and ambient noise filtration capabilities, we could perform experiments on diverse images, including scenes such as a chair on a lawn, an office, and a mulch palette. Although there are datasets from the Kinect v2 sensor that offer aligned RGB and depth images, due to the sensors’ internal post-processing pipeline, the flying pixels are identified and removed from the depth map [21]. Therefore, the Kinect datasets are unsuitable for studying flying pixel artifacts.

Our experiments with the *Oyla* dataset yield promising results. As demonstrated in Figure 7, our method accurately corrects flying pixels, aligning them with the surfaces of their respective objects while preserving both structure and color. Even in cases where the distance between a flying pixel and its correct object is considerable, our method maintains accuracy, as seen in both the chair and room scenes. Overall, there is a significant reduction in flying pixels in *Oyla* data.

It is important to note that some pixels may still appear flying after correction. This issue arises when there is minimal color variation between foreground and background objects within the field of view, resulting in insufficient filtering of objects (see Figure 7). Consequently, the new coordinates of the flying pixels become an average of the two objects’ depths, leading to inaccurate corrections. Since our method relies heavily on color information, flying pixels between objects of homogeneous colors will likely be left uncorrected. In such cases, removing the FP may be ideal since the color information is not sufficiently discriminative.

²https://github.com/ekamresh/oyla_datasets

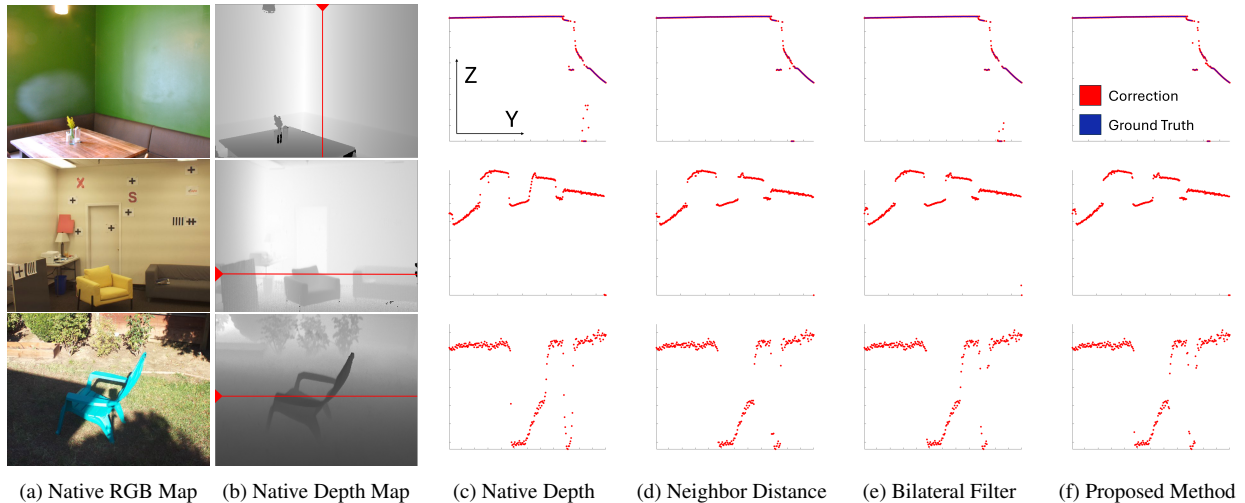


Fig. 6: Comparison of selected algorithms on both real and ground-truth data. Horizontal and vertical slices of depth map are taken to compare the result of correction by various methods.

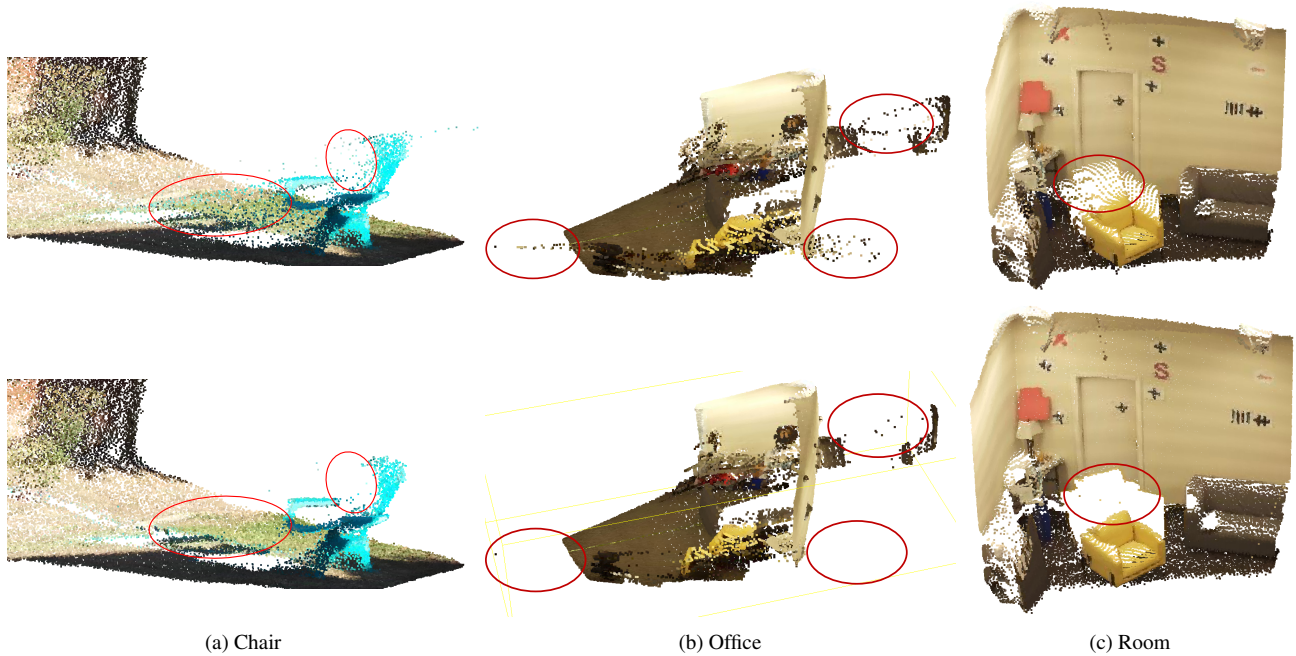


Fig. 7: Qualitative evaluation of proposed correction algorithm on *Oyla* dataset. Point clouds obtained from aligned RGB and depth images before (top) and after (bottom) correction are shown

5. CONCLUSION

We propose a novel method for correcting flying pixels, leveraging 3D neighborhoods around FPs and a high-resolution color prior. Both visual inspection and quantitative analysis using a synthetic dataset demonstrate a significant reduction in flying pixels. The qualitative assessment shows that corrected pixels align more accurately with actual surfaces. At the same time, quantitative analysis confirms an improved estimation of a flying pixel’s true value relative to a ground truth. The proposed method performs well against other modes of flying pixel correction. This approach enhances the

quality of depth maps generated by ToF cameras, improving the reliability and accuracy of downstream tasks.

Future work may focus on using the physical properties of the camera, e.g., pixel FoV with FPs, to correct other systemic issues seen within depth cameras. Additionally, improving upon the hardware setup seen within the *Oyla* camera to generate even higher resolution, better aligned data would be beneficial to correcting such errors.

6. REFERENCES

- [1] Ilya Chugunov, Seung-Hwan Baek, Qiang Fu, Wolfgang Heidrich, and Felix Heide. Mask-tof: Learning microlens masks for flying pixel correction in time-of-flight imaging. *The IEEE Conference on Computer Vision and Pattern Recognition (CVPR)*, 2021.
- [2] James Diebel and Sebastian Thrun. An application of markov random fields to range sensing. In Y. Weiss, B. Schölkopf, and J. Platt, editors, *Advances in Neural Information Processing Systems*, volume 18. MIT Press, 2005.
- [3] Paolo Favaro. Recovering thin structures via nonlocal-means regularization with application to depth from defocus. In *2010 IEEE Computer Society Conference on Computer Vision and Pattern Recognition*, pages 1133–1140, 2010.
- [4] Sobers L. X. Francis, Sreenatha G. Anavatti, Matthew A. Garratt, and Hyun-Sik Shim. A tof-camera as a 3d vision sensor for autonomous mobile robotics. *International Journal of Advanced Robotic Systems*, 12, 2015.
- [5] Stefan Fuchs and Stefan May. Calibration and registration for precise surface reconstruction with tof cameras. In *Proceedings of the Dynamic 3D Imaging Workshop in Conjunction with DAGM (Dyn3D)*, volume 1, 2007.
- [6] Vijaya K. Ghorpade, Paul Checchin, and Laurent Trassoudaine. Line-of-sight-based tof camera’s range image filtering for precise 3d scene reconstruction. In *2015 European Conference on Mobile Robots (ECMR)*, pages 1–6, 2015.
- [7] Yu He and Shengyong Chen. Recent advances in 3d data acquisition and processing by time-of-flight camera. *IEEE Access*, 7:12495–12510, 2019.
- [8] Peter Henry, Michael Krainin, Evan V. Herbst, Xiaofeng Ren, and Dieter Fox. Rgb-d mapping: Using depth cameras for dense 3d modeling of indoor environments. In *International Symposium on Experimental Robotics*, 2010.
- [9] Benjamin Huhle, Philipp Jenke, and Wolfgang Straßer. On-the-fly scene acquisition with a handy multi-sensor system. *International Journal of Intelligent Systems Technologies and Applications*, 5(3-4):255–263, 2008.
- [10] Tobias Koch, Lukas Liebel, Marco Körner, and Friedrich Fraundorfer. Comparison of monocular depth estimation methods using geometrically relevant metrics on the ibims-1 dataset. *Computer Vision and Image Understanding (CVIU)*, 191:102877, 2020.
- [11] Johannes Kopf, Michael F Cohen, Dani Lischinski, and Matt Uyttendaele. Joint bilateral upsampling. *ACM Transactions on Graphics (ToG)*, 26(3):96–es, 2007.
- [12] Johannes Kopf, Michael F. Cohen, Dani Lischinski, and Matt Uyttendaele. Joint bilateral upsampling. *ACM Trans. Graph.*, 26(3):96–es, jul 2007.
- [13] Marek Kraft, Michał Nowicki, Rudi Penne, Adam Schmidt, and Piotr Skrzypczyński. Efficient rgb–d data processing for feature–based self–localization of mobile robots. *International Journal of Applied Mathematics and Computer Science*, 26, 03 2016.
- [14] R. Lange and P. Seitz. Solid-state time-of-flight range camera. *IEEE Journal of Quantum Electronics*, 37(3):390–397, 2001.
- [15] Hiroaki Niitsuma and Tsutomu Maruyama. Sum of absolute difference implementations for image processing on fpgas. In *2010 International Conference on Field Programmable Logic and Applications*, pages 167–170, 2010.
- [16] Jaesik Park, Hyeongwoo Kim, Yu-Wing Tai, Michael S. Brown, and In So Kweon. High-quality depth map upsampling and completion for rgb-d cameras. *IEEE Transactions on Image Processing*, 23(12):5559–5572, 2014.
- [17] Kaustubh Pathak, Andreas Birk, and Jann Poppinga. Sub-pixel depth accuracy with a time of flight sensor using multimodal gaussian analysis. In *2008 IEEE/RSJ International Conference on Intelligent Robots and Systems*, pages 3519–3524, 2008.
- [18] Xin Qiao, Chenyang Ge, Huimin Yao, Pengchao Deng, and Yanhui Zhou. Valid depth data extraction and correction for time-of-flight camera. In *Twelfth International Conference on Machine Vision (ICMV 2019)*, volume 11433, pages 696–703. SPIE, 2020.
- [19] Malcolm Reynolds, Jozef Doboš, Leto Peel, Tim Weyrich, and Gabriel J Brostow. Capturing time-of-flight data with confidence. In *CVPR 2011*, pages 945–952, 2011.
- [20] Alexander Sabov and Jörg Krüger. Identification and correction of flying pixels in range camera data. In *Proceedings of the 24th Spring Conference on Computer Graphics, SCCG ’08*, page 135–142, New York, NY, USA, 2008. Association for Computing Machinery.
- [21] Hamed Sarbolandi, Damien Lefloch, and Andreas Kolb. Kinect range sensing: Structured-light versus time-of-flight kinect. *Computer Vision and Image Understanding*, 139:1–20, 2015.
- [22] Spickermann, Ralph and Singh, Raghavendra and Kalluri, Srinath. Device and method of object detection. Patent US11455710B2, Septemeber 2022.
- [23] Michal Tölgyessy, Martin Dekan, L’uboš Chovanec, and Peter Hubinský. Evaluation of the azure kinect and its comparison to kinect v1 and kinect v2. *Sensors*, 21(2):413, 2021.
- [24] Hongshan Yu, Jiang Zhu, Yaonan Wang, Wenyan Jia, Mingui Sun, and Yandong Tang. Obstacle classification and 3d measurement in unstructured environments based on tof cameras. *Sensors*, 14(6):10753–10782, 2014.